PHYSICAL REVIEW B VOLUME 44, NUMBER 15 15 OCTOBER 1991-I

Quantum point contacts in magnetic fields

T. Ando
Institute for Solid State Physics, University of Tokyo, 7-22-1 Roppongi, Minato-ku, Tokyo 106, Japan
(Received 9 January 1991)

A method is described for the numerical calculations of the ballistic conductance in mesoscopic structures in magnetic fields within a lattice model. Examples of calculated results are given for the conductance across a single quantum point contact and a series of two quantum point contacts. The conductance is quantized even when the confinement is not adiabatic and interchannel scatterings are still appreciable. The quantization becomes better in magnetic fields. In a series of two quantum point contacts, the magnetic field dependence of the conductance is strongly dependent on the channel number of both emitter and collector contacts.

I. INTRODUCTION

Recent developments in microfabrication technology have made it possible to obtain quantum ballistic structures by introducing a confining potential in a two-dimensional electron system, typically by lithography techniques on modulation-doped $GaAs/Al_xGa_{1-x}As$ heterostructures. Various phenomena associated with the ballistic conduction have been observed at low temperatures. One of the most striking effects is the quantization of the conductance across a narrow constriction (quantum point contact).[1,2] Transport phenomena associated with wire junctions have also been observed, such as anomalies in the low-field Hall effect,[3–5] a bend resistance,[6] and a negative resistance.[7] The purpose of the present paper is to describe a numerical method of calculating the conductance in the ballistic regime in magnetic fields and present results for a single and a series of two point contacts.

The conductance quantization has been observed at point contacts made by a split-gate technique[1,2] and later also at constrictions made by focused ion beam scanning.[8] Effects of magnetic fields have been studied and shown to enhance the quantization.[9] Effects observed in combinations of several point contacts include nonadditivity of the conductance,[10–12] zero-dimensional states,[13,14] and focusing effects.[15–17] Quite recently, Okada *et al.*[18] measured the conductance across a series of two point contacts as a function of magnetic field and found an interesting dependence on the channel number of the source contact. They have observed a single peak as a function of the magnetic field for the case of a single channel and splitting into two peaks when the channel number is 2.

The quantization of the conductance into integer multiples of $e^2/\pi\hbar$ can be explained easily in an adiabatic, i.e., slowly varying, geometry. However, the actual systems may not completely be in such a limit. Various estimates of the corrections to the adiabatic limit have been reported.[19–22] Calculations have also been done based on an exactly soluble model[23] and numerically for model constrictions abruptly connected to wide regions.[24–29] These calculations have demonstrated the sensitivity of the conductance to the form of the confinement. Effects of magnetic fields have not been studied in detail except for some analytic considerations in the adiabatic case.[30,31]

There are various ways of calculating conductance in ballistic structures. Exact analytic solutions and their combinations[23] are possible in some cases but their applications are limited to special kinds of boundaries. A direct numerical integration of the Schrödinger equation is another candidate. The simplest way is to use a lattice model, i.e., a discretization of space. It is particularly convenient in the presence of a magnetic field which is incorporated simply in the form of a Peierls phase factor of the transfer integral. Further, it can straightforwardly be extended to the study of effects of scattering from impurities. It has been used, for example, in calculating ballistic transport associated with junctions of quantum wires.[32,33]

In this paper, we introduce a confining potential in a square lattice and calculate the conductance across a single point contact and a series of two point contacts in magnetic fields. In Sec. II, the procedure to calculate the conductance of ballistic structures in the lattice model is briefly described. Although the method itself is well established in the absence of a magnetic field, there are some nontrivial aspects especially with respect to scattering problems in magnetic fields. This method is based on three essential ingredients: Landauer's conductance formula, the relation of transmission coefficients to the Green function, and a recursive calculation of the Green function. In Sec. III the conductance is explicitly calculated in a model quantum point contact in magnetic fields both in the absence and presence of scatterers. In Sec. IV numerical calculations are performed on a series of two point contacts. It will be demonstrated that the magnetic-field dependence of the conductivity is strongly modified by the channel number of the emitter and collector point contacts, i.e., the channel wave functions are directly reflected in the conductance. The summary and conclusion are given in Sec. V.

II. CONDUCTANCE CALCULATION IN A LATTICE MODEL

A. Hamiltonian

We consider a square lattice with lattice constant a and an isotropic nearest-neighbor transfer integral $-t$. The lattice point is specified as (l,j). A magnetic field H is included in terms of a Peierls phase factor of the transfer integral. We choose the gauge such that

$$\langle l,j|\mathcal{H}|l+1,j\rangle=-t\exp(2\pi i\tilde{H}j)\quad\langle l,j|\mathcal{H}|l,j+1\rangle=-t\ , \tag{2.1}$$

where $\tilde{H}=\Phi/\Phi_0$ with $\Phi=Ha^2$ being the magnetic flux passing through a unit cell and $\Phi_0=ch/e$ being the magnetic flux quantum. The diagonal element of the Hamiltonian is chosen to be

$$\langle l,j|\mathcal{H}|l,j\rangle=4t+v(l,j)\ , \tag{2.2}$$

where the first term on the right-hand side shifts the energy origin to the bottom of the band and the second term represents the potential energy including that of the confinement.

In the following, we measure almost all quantities in units of corresponding quantities in two dimensions, i.e., energy is measured in units of the Fermi energy E_F and length in units of the Fermi wavelength λ_F. The resonance energy appearing in the lattice model is obtained as

$$t=E_F\left[\frac{1}{2\pi}\right]^2\left[\frac{\lambda_F}{a}\right]^2\ . \tag{2.3}$$

The magnetic field is given by

$$\tilde{H}=\frac{a^2}{R_c\lambda_F}=\pi\frac{\hbar\omega_c}{E_F}\left[\frac{a}{\lambda_F}\right]^2\ , \tag{2.4}$$

with $\omega_c=eH/mc$ the cyclotron frequency and $R_c=v_F/\omega_c$ the classical cyclotron radius, where v_F is the Fermi velocity.

Effects of scattering are introduced through randomness of site energy $v(l,j)$ distributed uniformly with width W [$v(l,j)\rightarrow v(l,j)+w(l,j)$ with $-W/2<w(l,j)<W/2$]. The model corresponds to a system containing a high concentration of scatterers with δ potential. In terms of the mean free path Λ in two dimensions, we have

$$\frac{W}{E_F}=\left[\frac{6\lambda_F^3}{\pi^3a^2\Lambda}\right]^{1/2}\ . \tag{2.5}$$

B. Ideal wire

First we shall consider a wire infinitely long in the x direction and consisting of M lattice sites in the y direction. For $a\ll\lambda_F$, this simulates a continuum system with width $(M+1)a$. The equation of motion can be written as

$$(E-\mathcal{H}_0)\mathbf{C}_j+tP\mathbf{C}_{j-1}+tP^*\mathbf{C}_{j+1}=\mathbf{0}\ , \tag{2.6}$$

where $\mathbf{C}_j$ is a vector describing the amplitudes of the jth cell consisting of M sites and P is an $M\times M$ matrix consisting of phase factors:

$$P_{ll'}=\exp(2\pi i\tilde{H}l)\delta_{l,l'}\quad(l,l'=1,\ldots,M)\ . \tag{2.7}$$

The Hamiltonian $\mathcal{H}_0$ is an $M\times M$ matrix given by

$$\mathcal{H}_0=\begin{bmatrix} v_1+4t & -t & 0 & \cdots & 0 \\ -t & v_2+4t & -t & \cdots & 0 \\ 0 & -t & v_3+4t & \cdots & 0 \\ \vdots & \vdots & \vdots & \ddots & \vdots \\ 0 & 0 & 0 & \cdots & v_M+4t \end{bmatrix}\ , \tag{2.8}$$

with v_l being the local potential energy at the site l.

To obtain linearly independent solutions for Eq. (2.6) we first set

$$\mathbf{C}_j=\lambda^j\mathbf{C}_0\ . \tag{2.9}$$

Substituting this into Eq. (2.6) we have

$$\lambda\mathbf{C}_j=t^{-1}P(\mathcal{H}_0-E)\mathbf{C}_j-P^2\mathbf{C}_{j-1}\ , \tag{2.10}$$

which combined with

$$\lambda\mathbf{C}_{j-1}=\mathbf{C}_j \tag{2.11}$$

leads to the following eigenvalue problem:

$$\lambda\begin{bmatrix}\mathbf{C}_j\\ \mathbf{C}_{j-1}\end{bmatrix}=\begin{bmatrix}t^{-1}P(\mathcal{H}_0-E) & -P^2\\ 1 & 0\end{bmatrix}\begin{bmatrix}\mathbf{C}_j\\ \mathbf{C}_{j-1}\end{bmatrix}\ . \tag{2.12}$$

The wave number k is related to the eigenvalue λ through

$$\exp[ika+i\pi\tilde{H}(M+1)]=\lambda\ . \tag{2.13}$$

This equation has $2M$ eigenvalues and $2M$ eigenvectors, which are classified into M right- and left-going waves. The M right-going solutions consist of traveling waves with velocity in the positive x direction and evanescent waves decaying exponentially in the positive x direction. Similarly, the M left-going solutions consist of traveling waves with velocity in the negative x direction and evanescent waves decaying exponentially in the negative x direction. In general, any solutions of Eq. (2.6) can be represented by a linear combination of these eigensolutions.

Let $\mathbf{u}_1(-),\ldots,\mathbf{u}_M(-)$ be $\mathbf{C}_0$ of the left-going solutions corresponding to $\lambda_1(-),\ldots,\lambda_M(-)$ and $\mathbf{u}_1(+),\ldots,\mathbf{u}_M(+)$ be $\mathbf{C}_0$ of the right-going solutions corresponding to $\lambda_1(+),\ldots,\lambda_M(+)$. Define

$$U(\pm)=(\mathbf{u}_1(\pm)\cdots\mathbf{u}_M(\pm)) \tag{2.14}$$

and

$$\Lambda(\pm)=\begin{bmatrix}\lambda_1(\pm) & & \\ & \ddots & \\ & & \lambda_M(\pm)\end{bmatrix}\ . \tag{2.15}$$

Any left- and right-going waves are written, at $j=0$, for example, as

$$\mathbf{C}_0(\pm)=U(\pm)\mathbf{C}(\pm)\ , \tag{2.16}$$

where $\mathbf{C}(\pm)$ is an appropriate vector consisting of expansion coefficients. For general j we have

$$\mathbf{C}_j(\pm)=U(\pm)\Lambda(\pm)^j\mathbf{C}(\pm)\ , \tag{2.17}$$

which leads to the relation

$$\mathbf{C}_j(\pm)=F(\pm)^{j-j'}\mathbf{C}_{j'}(\pm)\ , \tag{2.18}$$

with

$$F(\pm)=U(\pm)\Lambda(\pm)U^{-1}(\pm)\ . \tag{2.19}$$

Note that $U(\pm)$ is in general not a unitary matrix.

C. Scattering problem

Now let us consider the scattering problem for the wire with length N (from cell 1 to cell N) to both sides of which an ideal wire is attached. First, we separate the amplitude $\mathbf{C}_0$ at cell 0 into the right-going (incident) and left-going (reflected) solutions:

$$\mathbf{C}_0=\mathbf{C}_0(+)+\mathbf{C}_0(-)\ . \tag{2.20}$$

Using Eq. (2.19), the amplitude at cell -1 is written as

$$\mathbf{C}_{-1}=F^{-1}(+)\mathbf{C}_0(+)+F^{-1}(-)\mathbf{C}_0(-)\ . \tag{2.21}$$

This gives

$$\mathbf{C}_{-1}=F^{-1}(-)\mathbf{C}_0+[F^{-1}(+)-F^{-1}(-)]\mathbf{C}_0(+)\ . \tag{2.22}$$

Therefore, the equation of motion at cell 0 becomes

$$(E-\tilde{\mathcal{H}}_0)\mathbf{C}_0+tP^*\mathbf{C}_1 =-tP[F^{-1}(+)-F^{-1}(-)]\mathbf{C}_0(+)\ , \tag{2.23}$$

with

$$\tilde{\mathcal{H}}_0=\mathcal{H}_0-tPF^{-1}(-)\ . \tag{2.24}$$

Note that $\tilde{\mathcal{H}}_0$ is not Hermitian.

On the other hand, only right-going (out-going) waves can exist at cell $N+1$. Therefore, we have

$$\mathbf{C}_{N+2}=F(+)\mathbf{C}_{N+1}\ , \tag{2.25}$$

which gives the equation of motion at cell $N+1$

$$(E-\tilde{\mathcal{H}}_{N+1})\mathbf{C}_{N+1}+tP\mathbf{C}_N=0\ , \tag{2.26}$$

with

$$\tilde{\mathcal{H}}_{N+1}=\mathcal{H}_{N+1}-tP^*F(+)\ . \tag{2.27}$$

Note that $\mathcal{H}_{N+1}=\mathcal{H}_0$ and that $\tilde{\mathcal{H}}_{N+1}$ is not Hermitian.

Define the Green function G as

$$G=\frac{1}{E-\tilde{\mathcal{H}}} \tag{2.28}$$

with

$$\tilde{\mathcal{H}}=\begin{bmatrix} \tilde{\mathcal{H}}_0 & -tP^* & 0 & \cdots & 0 & 0 \\ -tP & \tilde{\mathcal{H}}_1 & V & \cdots & 0 & 0 \\ 0 & -tP & \tilde{\mathcal{H}}_2 & \cdots & 0 & 0 \\ \vdots & \vdots & \vdots & \ddots & \vdots & \vdots \\ 0 & 0 & 0 & \cdots & \tilde{\mathcal{H}}_N & -tP^* \\ 0 & 0 & 0 & \cdots & -tP & \tilde{\mathcal{H}}_{N+1} \end{bmatrix}\ , \tag{2.29}$$

where $\tilde{\mathcal{H}}_j=\mathcal{H}_j$ for $j=1,2,\ldots,N$. Immediately, we can derive

$$\mathbf{C}_{N+1}(+)=\mathbf{C}_{N+1} =-t(N+1|G|0)P[F^{-1}(+)-F^{-1}(-)]\mathbf{C}_0(+) \tag{2.30}$$

and

$$\mathbf{C}_0(-)=\mathbf{C}_0-\mathbf{C}_0(+) =\{-t(0|G|0)P[F^{-1}(+)-F^{-1}(-)]-1\}\mathbf{C}_0(+)\ . \tag{2.31}$$

From these equations we can obtain the transmission coefficient $t_{\mu\nu}$ for the incident channel ν with velocity v_ν and out-going channel μ with velocity v_μ as

$$t_{\mu\nu}=\left[\frac{v_\mu}{v_\nu}\right]^{1/2}\{-tU^{-1}(+)(N+1|G|0) \times P[F^{-1}(+)-F^{-1}(-)]U(+)\}_{\mu\nu} \tag{2.32}$$

and the reflection coefficient $r_{\mu\nu}$ for incident channel ν and out-going channel μ as

$$r_{\mu\nu}=\left[\frac{v_\mu}{v_\nu}\right]^{1/2}(U^{-1}(-)\{-t(0|G|0)P[F^{-1}(+)-F^{-1}(-)]-1\}U(+))_{\mu\nu}\ . \tag{2.33}$$

In the absence of a magnetic field, these formulas reduce to the simpler expressions[34–36] widely used in various numerical studies. In terms of the transmission coefficient $t_{\mu\nu}$, the conductance G is given by the multichannel version[34] of Landauer's formula:[37]

$$G=\frac{e^2}{\pi\hbar}\sum_{\mu\nu}|t_{\mu\nu}|^2\ . \tag{2.34}$$

To calculate the Green function, we define the diagonal and off-diagonal Green functions by

$$\begin{aligned}(j|G^{(j)}|j)^{-1}&=[j|(E-\mathcal{H}^{(j)})^{-1}|j]\ ,\\ (j|G^{(j)}|0)^{-1}&=[j|(E-\mathcal{H}^{(j)})^{-1}|0]\ ,\end{aligned} \tag{2.35}$$

where $\mathcal{H}^{(j)}$ is the total Hamiltonian for the strip comprising the 0 to j cells excluding the intercell Hamiltonian

$\tilde{\mathcal{H}}_{j,j+1}$ and $\tilde{\mathcal{H}}_{j+1,j}$. Then, the Green function for strips with any length can be obtained by a set of recursive formulas,[38-45]

$$(j+1|G^{(j+1)}|j+1)^{-1} = E-\tilde{\mathcal{H}}_{j+1}-\tilde{\mathcal{H}}_{j+1,j}(j|G^{(j)}|j)\tilde{\mathcal{H}}_{j,j+1} , \quad (2.36)$$

$$(j+1|G^{(j+1)}|0) = (j+1|G^{(j+1)}|j+1)\mathcal{H}_{j+1,j}(j|G^{(j)}|0) ,$$

with the initial condition $(0|G^{(0)}|0)=(E-\tilde{\mathcal{H}}_0)^{-1}$. Note that $-t^{-1}F^{-1}(-)P$ and $-t^{-1}F(+)P^*$ are the diagonal Green function under the boundary condition of left- and right-going waves, respectively.[46]

III. SINGLE POINT CONTACT

A. Model

We consider a wire with length L_x and width L_y ($-L_x/2<x<L_x/2$ and $-L_y/2<y<L_y/2$) and introduce the following potential which confines electron motion in the y direction in the vicinity of the center of the wire:

$$V(x,y)=\frac{V}{2}\left[1+\cos\left[\frac{2\pi x}{L_x}\right]\right] + E_F\sum_{\pm}\left[\frac{y-y_{\pm}(x)}{\Delta}\right]^2\Theta(y^2-y_{\pm}(x)^2) , \quad (3.1)$$

where $\theta(t)$ is a step function, defined by $\theta=1$ for $t>0$ and $\theta=0$ otherwise, and

$$y_{\pm}(x)=\pm\frac{L_y}{4}\left[1-\cos\left[\frac{2\pi x}{L_x}\right]\right] . \quad (3.2)$$

The parameter Δ/λ_F characterizes the width of the channel of the point contact and V represents the maximum bottom energy at $x=y=0$. For a fixed width L_y, the wire length L_x determines the length scale over which the potential varies. The adiabatic limit corresponds to $L_x/\lambda_F \gg 1$.

At $x=0$ the confining potential is parabolic. With increasing distance from $x=0$, the bottom energy decreases and at the same time the effective width becomes larger. This model is expected to simulate the potential variation in the vicinity of actual quantum point contacts for appropriate values of the parameters. The potential profile for $\Delta/\lambda_F=1$, $L_y/\lambda_F=4$, and $V/E_F=0.5$ is given in Fig. 1.

B. Numerical results

Figure 2 gives examples of the calculated conductance across the point contact for $L_x/\lambda_F=4$, 8, and 16. The other parameters are the same as in Fig. 1. For $L_x/\lambda_F=4$ the potential variation is far from being adiabatic and the conductance is not quantized. With the increase of the magnetic field, however, it becomes well quantized. This is because the magnetic field creates edge

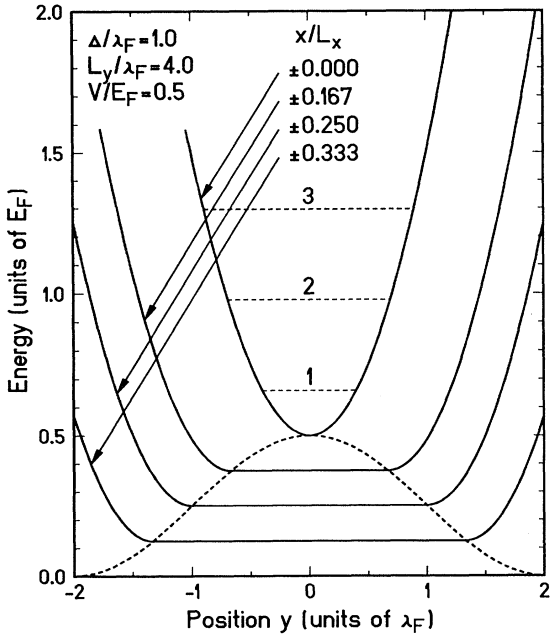

FIG. 1. An example of the potential profile at a quantum point contact for $V/E_F=0.5$, $\Delta/\lambda_F=1$, and $L_y/\lambda_F=4$. The solid lines represent the potential at $x/L_x=0$, $\pm1/6$, $\pm1/4$, and $\pm1/3$ as a function of y. The horizontal dashed lines represent the bottom of the one-dimensional subbands at the contact, i.e., for the parabolic potential at $x=0$.

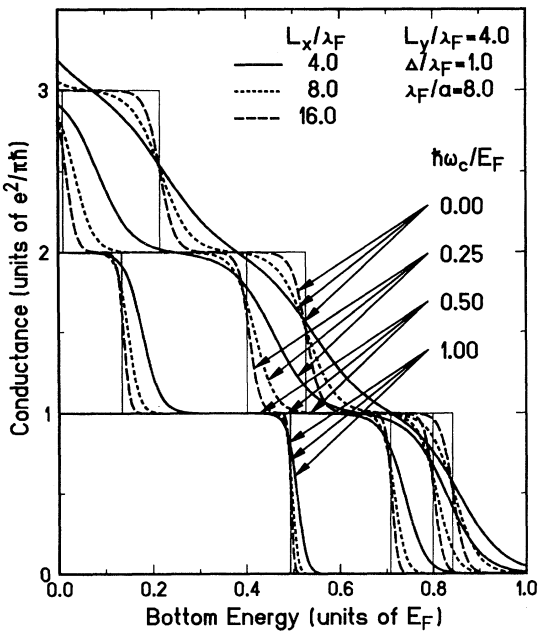

FIG. 2. Examples of the calculated conductance across a quantum point contact as a function of the bottom energy V in magnetic fields. The thin straight lines represent the channel number at the contact. When the confinement potential varies more slowly, the conductance quantization becomes better.

states and reduces backscattering considerably. For $L_x/\lambda_F=16$ we can see a well-developed conductance quantization even in the absence of a magnetic field.

Figure 3 gives the current distribution G_μ for the out-going or incoming channels, defined by

$$G_\mu=\frac{e^2}{\pi\hbar}\sum_\nu |t_{\mu\nu}|^2=\frac{e^2}{\pi\hbar}\sum_\nu |t_{\mu\nu}|^2 , \tag{3.3}$$

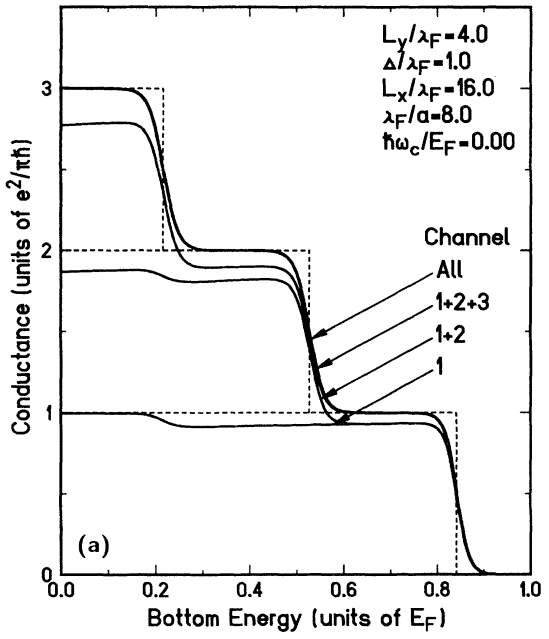

FIG. 3. Examples of the calculated current distribution among out-going channels as a function of the bottom energy V when the conductance is well quantized. Most of the current is carried by the out-going channel identical to that at the point contact because of the adiabatic nature of the potential, but contributions of other channels are still noticeable. (a) $L_x/\lambda_F=16$ and $\hbar\omega_c/E_F=0$, (b) $L_x/\lambda_F=8$ and $\hbar\omega_c/E_F=0.25$.

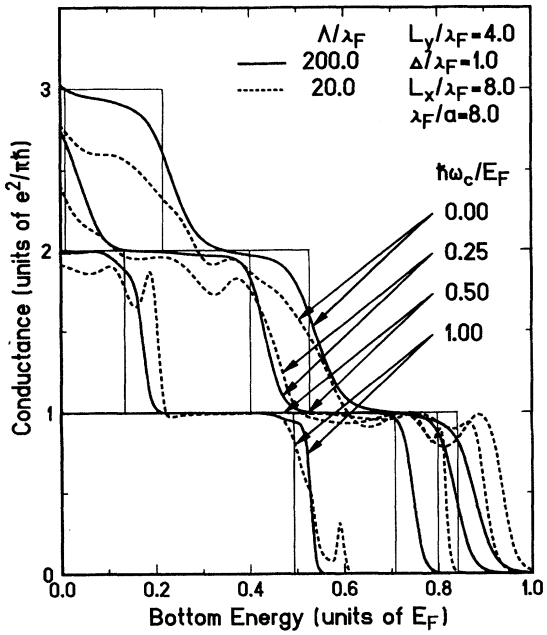

FIG. 4. Examples of the calculated conductance across a quantum point contact as a function of the bottom energy V in the presence of short-range randomness characterized by the mean free path Λ. The thin straight lines represent the channel number at the contact.

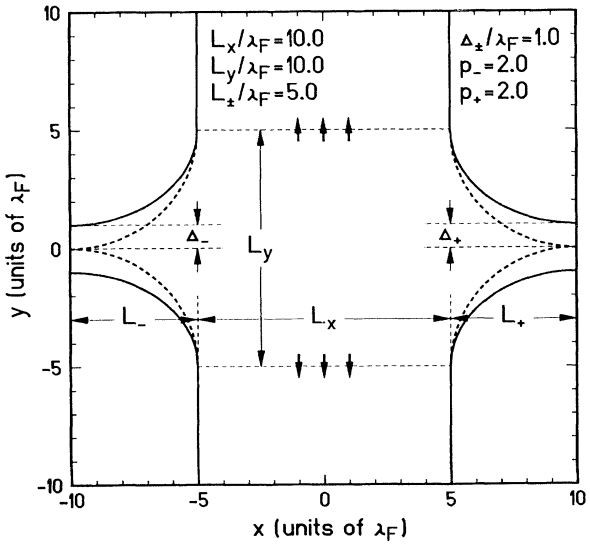

FIG. 5. A schematic illustration of a series of two quantum point contacts. Electrons are injected from the emitter point contact on the left-hand side and collected by the collector contact on the right-hand side. In the central region, both top and bottom edges are connected to an ideal and infinitely long wire. We define L_x as the width of the wire in the y direction (width of the region without confinement potential), $L_\pm$ as the length over which the confining potential varies in the emitter and collector contacts, and L_y as the width of the opening. At the point contacts, the bottom of the parabolic confinement potential $V_\pm$ can be raised in order to control the channel number. The parameters characterizing the confinement potential at the point contacts are $p_\pm=2$, $\Delta_\pm/\lambda=1$, $L_\pm/\lambda_F=5$, $L_x/\lambda_F=10$, and $L_y/\lambda_F=10$.

for the two cases where the conductance is well quantized [(a) $L_x/\lambda_F=16$ at $\hbar\omega_c/E_F=0$ and (b) $L_x/\lambda_F=8$ at $\hbar\omega_c/E_F=0.25$]. It should be noted that an appreciable part of the current is carried by channels different from those at the point contact although the total conductance is well quantized. In Fig. 3(a), for example, about 90% of the current is carried by channel 1 and the remaining $\sim 10\%$ is carried by channel 3 having the same symmetry for $0.6 \lesssim V/E_F \lesssim 0.8$. Such symmetry is destroyed by magnetic fields. Figure 3(b) shows that about 95% of the current is carried by the lowest channel and the remaining $\sim 5\%$ is carried by the first excited channel for $0.5 \lesssim V/E_F \lesssim 0.7$. Interchannel as well as intrachannel scatterings due to nonadiabaticity of the confining potential have been shown to be exponentially small in the slowly varying case.[19,20] Therefore, the present result shows that the conductance is quantized even when the potential is far from being in the adiabatic limit.

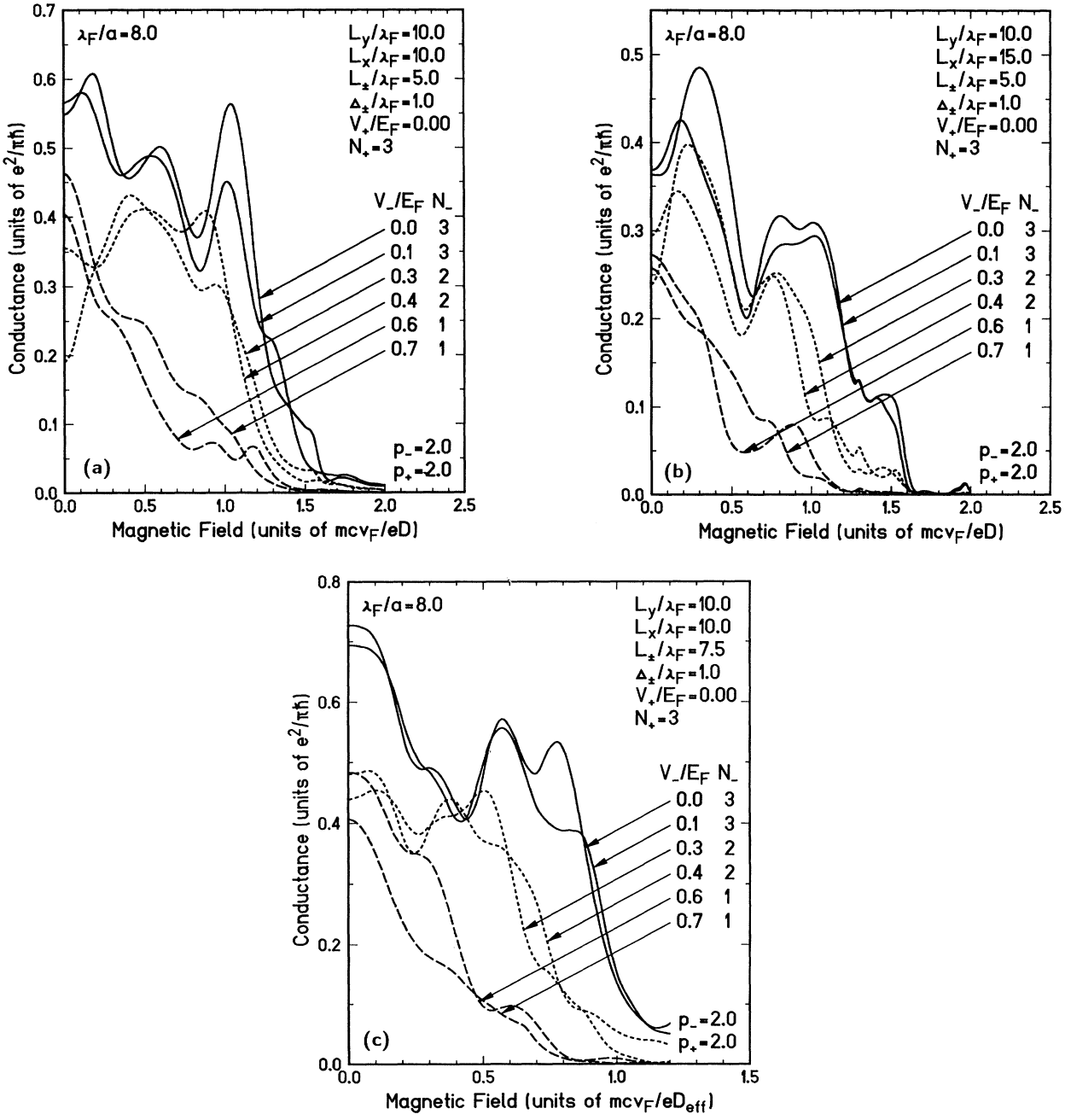

FIG. 6. Examples of the calculated conductance across a series of two quantum point contacts as a function of the magnetic field when the channel number of the collector contact is 3. The parameters are $L_y/\lambda_F=10$, $p_\pm=2$, and $\Delta_\pm/\lambda=1$. (a) $L_x/\lambda_F=10$ and $L_\pm/\lambda_F=5$, (b) $L_x/\lambda_F=15$ and $L_\pm/\lambda_F=5$, (c) $L_x/\lambda_F=10$ and $L_\pm/\lambda_F=7.5$.

Examples showing the effects of disorder are given in Fig. 4 for $L_x/\lambda_F=8$. Scattering modifies the quantization even when the mean free path is more than one order of magnitude larger than the length of the region where the confining potential is appreciable ($\Lambda/\lambda_F=200$). When Λ and L_x become comparable, the quantization is completely destroyed and the conductance exhibits fluctuations (a precursor of the universal conductance fluctuations). The randomness often gives rise to a sharp structure due to resonant tunneling through virtual bound states.

IV. SERIES OF TWO POINT CONTACTS

A. Model

To calculate the conductance for a series of two point contacts corresponding to recent experiments,[18] we shall use the model schematically shown in Fig. 5. At the boundaries $y=\pm L_y/2$, an infinitely long wire with width L_x is connected, i.e., we impose the boundary condition that only out-going waves are present at $y=\pm L_y/2$. The current is injected from the left (negative x direction) and collected by the right (positive x direction) point contact. The length of the region over which the confinement potential varies is L_- for the left and L_+ for the right contact. The outer ends of these point contacts are connected to infinitely long wires.

We first separate the region into three parts: the central region, the left emitter point-contact region, and the right collector point-contact region. The Green function is calculated from left to right in the emitter region and from right to left in the collector region. The Green function in the central part is calculated recursively from that of a small system near the center in a manner similar to that described by Eq. (2.36). This Green function is connected to that of outgoing ones and those of the emitter and collector point-contact regions at the outmost boundaries. The resulting Green function between the left and right edges can be used to calculate the corresponding transmission coefficients under the boundary conditions that only out-going waves exist at $y=\pm L_y/2$. Because electrons flow into the wires in the y direction the conductance between the two point contacts becomes smaller than $e^2/\pi\hbar$ especially in strong magnetic fields.

The confining potential at the point contact is simulated by the parabolic potential similar to that used in the single point-contact case discussed in the previous section. For example, the potential in the left point-contact region is given by

$$V(x,y)=\frac{V_-}{2}\left[1+\cos\left[\frac{\pi x}{L_-}\right]\right]+E_F\sum_{\pm}\left[\frac{y-y_{\pm}(x)}{\Delta(x)}\right]^2\Theta(y^2-y_{\pm}(x)^2)\ , \tag{4.1}$$

with

$$y_{\pm}(x)=\pm\frac{L_y}{2}\left[1-\left[\frac{x}{L_-}\right]^{p_-}\right]^{1/p_-}\ ,$$
$$\Delta(x)=\Delta_-\left[1-\left[\frac{x}{L_-}\right]^{p_-}\right]^{1/p_-}\ , \tag{4.2}$$

where the origin of x is chosen at the left edge. The similar potential is assumed in the collector region except

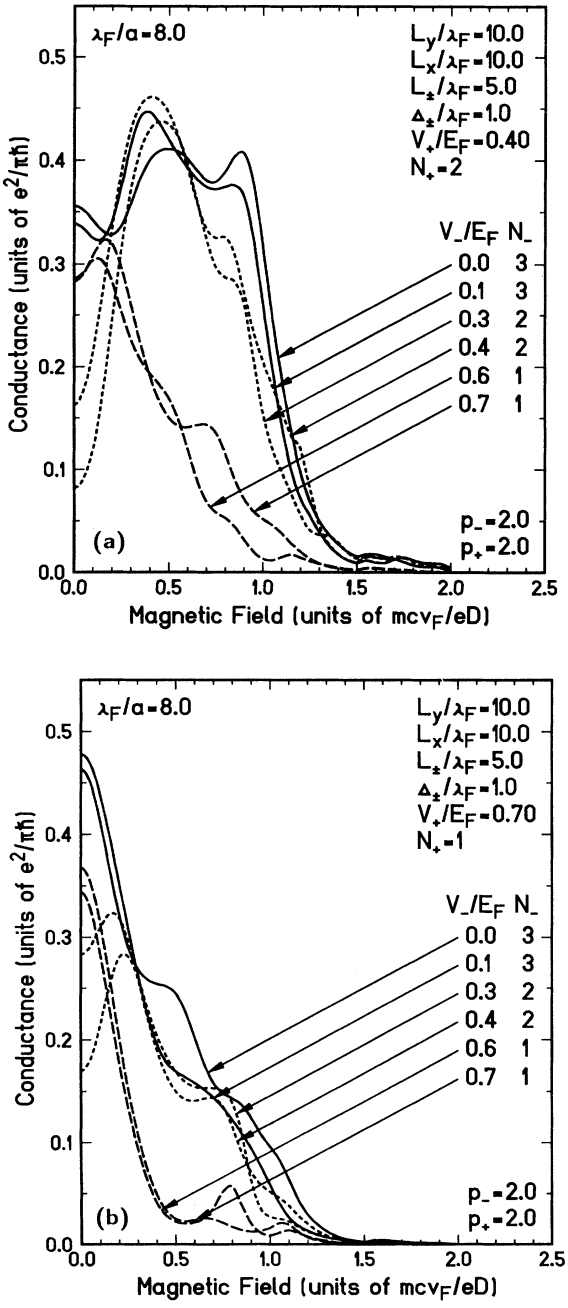

FIG. 7. Examples of the calculated conductance across a series of two quantum point contacts as a function of the magnetic field for $L_x/\lambda_F=L_y/\lambda_F=10$, $L_{\pm}/\lambda_F=5$, $p_{\pm}=2$, and $\Delta_{\pm}/\lambda=1$. (a) $N_+=2$ and (b) $N_+=1$.

that Δ_-, V_-, L_-, and p_- are replaced by Δ_+, V_+, L_+, and p_+, respectively.

B. Numerical results

Figure 6 gives examples of the calculated results when the channel number N_+ at the collector point contact is 3. The channel number N_- of the emitter point contact is varied by raising the bottom potential V_- at the left edge. The axis of abscissa is the ratio of the distance between the emitter and collector point contacts to the classical cyclotron radius, i.e., D/R_c with $D=L_x+L_++L_-$. In Fig. 6(a), the width of the region without confining potential is $L_x/\lambda_F=10$ and the length of the emitter and collector regions is $L_\pm/\lambda_F=5$. The flat region is wider in Fig. 6(b) and the point-contact region is wider in Fig. 6(c). In usual systems made on a $GaAs/Al_xGa_{1-x}As$ single heterostructure, the Fermi

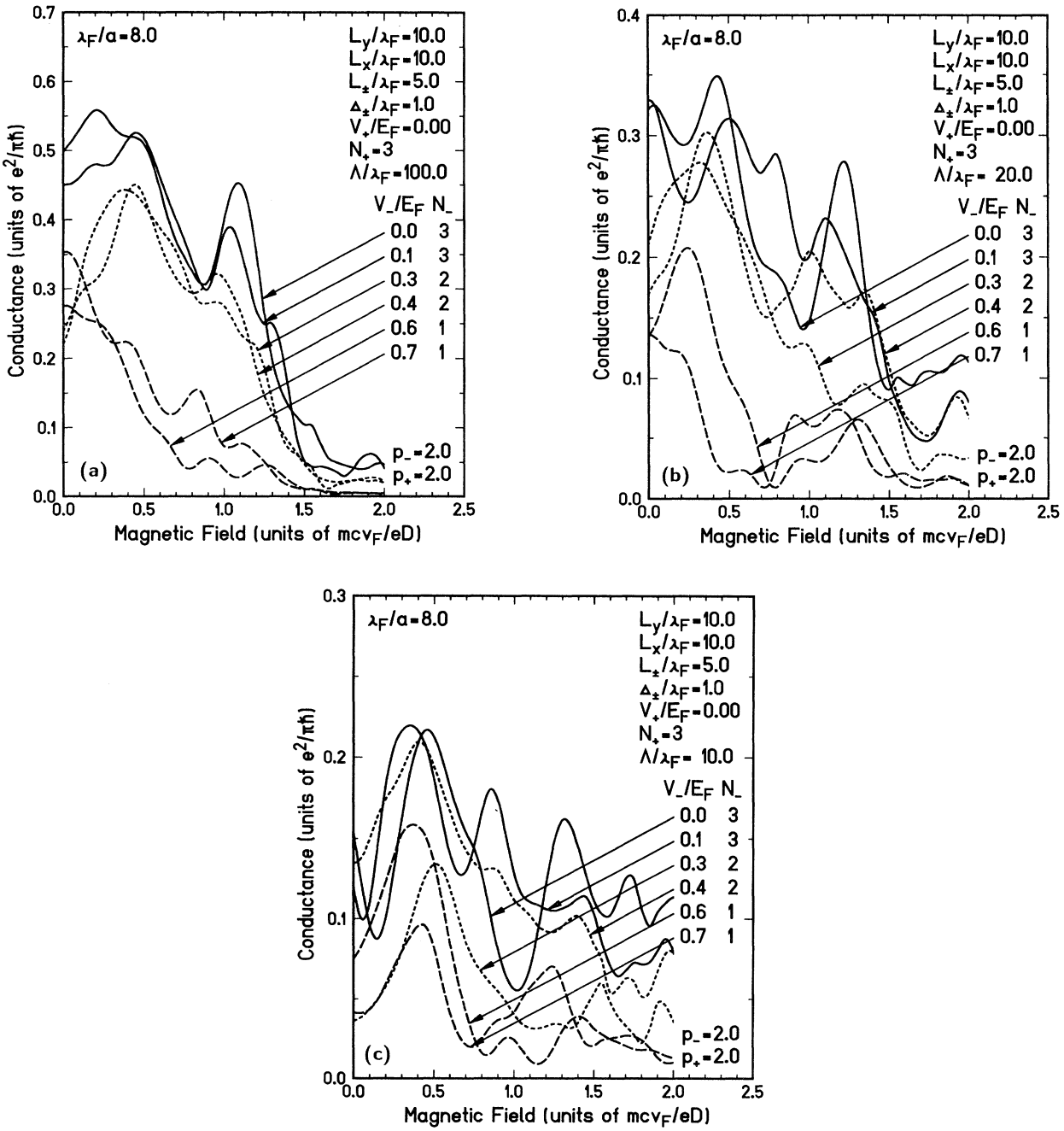

FIG. 8. Examples of the calculated conductance across a series of two quantum point contacts as a function of the magnetic field in the presence of scatterers with short-range potential. The parameters are $L_x/\lambda_F=L_y/\lambda_F=10$, $L_\pm/\lambda_F=5$, $p_\pm=2$, $\Delta_\pm/\lambda_F=1$, and $N_+=3$. (a) $\Lambda/\lambda_F=100$, (b) 20, and (c) 10.

wavelength is typically $\lambda_F \sim 500$ Å. Therefore, we have $D \sim 1$ μm and $L_y \sim 0.5$ μm, which are very close to the length scales of the point contacts used in the experiments.[18]

Oscillatory structures appear due to complex interferences with waves reflected from different parts of the boundaries.[47] Apart from these structures the conductance is determined essentially by the number of emitter channels. When there is a single channel in the emitter ($N_- = 1$), the conductance decays rapidly with increasing magnetic field. When the first excited channel is occupied, its contribution appears at higher magnetic fields. The difference between the conductance for $N_- = 3$ and 2 is large at weak magnetic fields, decreases, and then increases again with the magnetic field. These features are most clearly seen in Figs. 6(a) and 6(c). It can be concluded that the magnetic-field dependence of the conductance is determined essentially by the spatial (current) density distribution of the channels at the emitter point contact. This explains the recent experiments[18] which have shown that, for $N_+ = 3$, the conductance exhibits a single peak at zero magnetic field for $N_- = 1$ and a double peak as a function of magnetic field for $N_- = 2$. The fluctuations due to interference effects have not clearly been observed by the experiments, however.

The conductance depends also on the channel number of the collector point contact. Examples are given in Fig. 7, where $N_+ = 2$ in 7(a) and 1 in 7(b). As is shown in Fig. 7(a), when $N_+ = 2$, the difference of the conductance for $N_- = 1$ and 2 is still appreciable but the conductance remains essentially the same for $N_- = 2$ and 3. The same feature can be seen in Fig. 7(b). When $N_+ = 1$, the conductances for different N_+ are very close to each other although there remain slight differences. This interesting dependence on the collector channel has not been reported yet.

Examples showing effects of scattering are given in Fig. 8 for the same system shown in Fig. 6(a). Scattering modifies the conductance, particularly the interference patterns, even if the mean free path is about an order of magnitude larger than the distance D between the emitter and collector contacts ($\Lambda/\lambda_F = 100$) as shown in Fig. 8(a). When the mean free path becomes comparable to the distance [Fig. 8(b)], the original interference fluctuations disappear completely and new fluctuations appear due to scatterings from impurities. When $\Lambda < D$ [Fig. 8(c)], the conductance exhibits universal conductance fluctuations. These calculations show that the amplitude of the universal conductance fluctuations is larger than that due to complex interferences of waves reflected at different boundaries. It should be noted that the latter fluctuations are continuously taken over by the universal conductance fluctuations with the increase of the randomness.

At nonzero temperatures, we have to consider various effects which destroy the phase coherence of electrons. The first is averaging due to the broadening of the electron energy distribution. Examples of the results of such energy averaging are shown in Fig. 9. With increasing temperature the amplitude of the oscillatory structures decreases gradually. At high enough temperatures the interference fluctuations disappear completely and we can clearly identify the features corresponding to the channel wave functions. The energy broadening necessary to quench the fluctuations is estimated as $\Delta E/E_F \sim 2(\lambda_F/D)$ from the condition $\Delta k D \sim 2\pi$, which corresponds to the temperature of $k_B T/E_F \sim \Delta E/2\pi E_F \sim (1/\pi)(\lambda_F/D)$, in agreement with the numerical

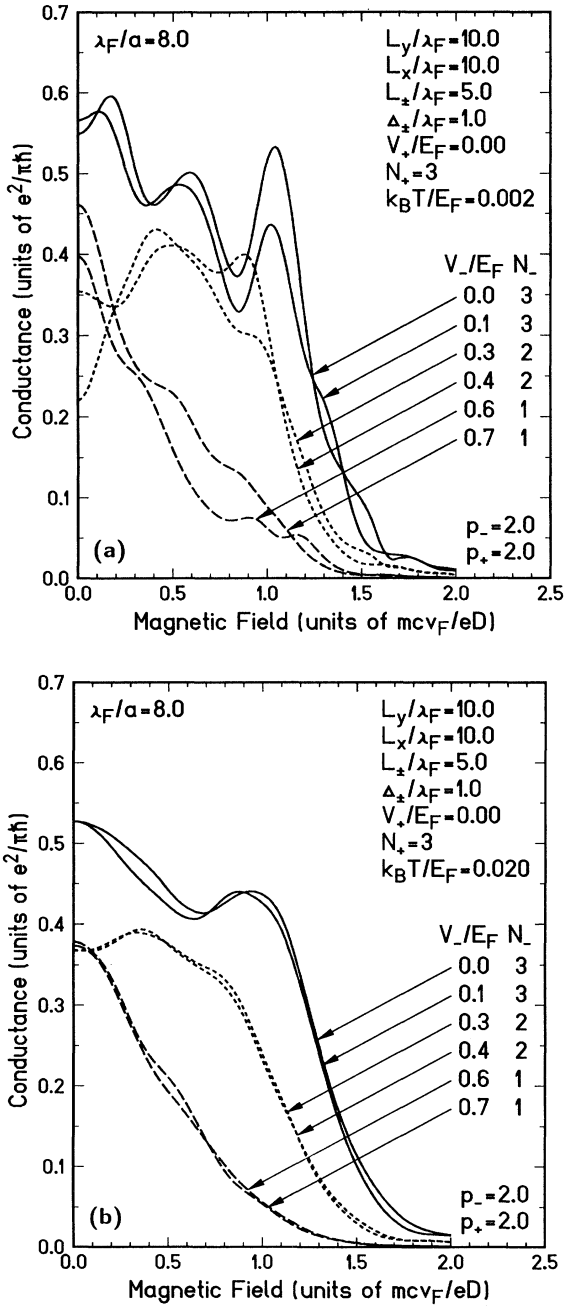

FIG. 9. Examples of the calculated conductance across a series of two quantum point contacts as a function of the magnetic field at nonzero temperatures. The parameters are $L_x/\lambda_F = L_y/\lambda_F = 10$, $L_\pm/\lambda_F = 5$, $p_\pm = 2$, $\Delta_\pm/\lambda_F = 1$, and $N_+ = 3$. (a) $k_B T/E_F = 0.002$ [roughly corresponding to experiments of Okada *et al.* (Ref. 18)] and (b) 0.02.

result. Another important effect is the inelastic scattering due to electron-electron and electron-phonon interactions. Calculations have been performed with the inclusion of a constant imaginary part in the site diagonal element of the Hamiltonian and given results quite similar to those at nonzero temperatures. Such calculations are certainly inappropriate because the imaginary part violates the current conservation, but might be sufficient for a qualitative description of the effects of inelastic scatterings on the interference fluctuations.

Numerical calculations have also been performed for $p_{\pm}$'s different from 2.0. The results show that the interference fluctuations are quite sensitive to the value of $p_{\pm}$. However, the characteristic features determined by the channel number of the emitter and collector point contacts remain the same as long as $p_{\pm}$ is not too different from 2.0 ($p_{\pm} \lesssim 4$).

V. SUMMARY AND CONCLUSION

A method of calculating the conductance in ballistic structures in magnetic fields has been discussed and examples of the numerical results have been presented. The model consists of a square lattice with effects of a magnetic field being included in the form of a Peierls phase factor. The conductance across a single point contact in magnetic fields has been explicitly calculated. It has been shown that the conductance becomes quantized even if the potential is not completely adiabatic and that the magnetic field tends to make the quantization better due to a reduction in the strength of back scattering at the point contact. The condition for the quantization is not necessarily $G_{\mu}=1$ or 0 as has frequently been discussed based on the adiabatic limit. Effects of scattering from impurities have been studied and shown to modify the quantization strongly even if the mean free path is much larger than the size of the point contact as expected.

The conductance across a series of two point contacts, similar to the system used in the experiments of Okada *et al.*,[18] has also been calculated. There appear fluctuations due to complex interferences of waves reflected from different boundaries. It has been shown that the magnetic-field dependence of the conductance is mainly determined by the density distribution of the narrow channel at the emitter point contact but depends also on the channel number of the collector point contact. The interference fluctuations are modified even in the presence of weak scattering from impurities and are gradually replaced by universal conductance fluctuations when scattering becomes strong.

ACKNOWLEDGMENTS

This work is supported in part by the Industry-University Joint Research Program "Mesoscopic Electronics" and by the Grant-in-Aid for Scientific Research on Priority Area "Electron Wave Interference Effects in Mesoscopic Structures" from the Ministry of Education, Science and Culture, Japan. I would like to thank M. Okada, M. Saito, and N. Yokoyama of Fujitsu Laboratories Ltd. for showing me their experimental results prior to publication.

[1]B. J. van Wees, H. van Houten, C. W. J. Beenakker, J. G. Williamson, L. P. Kouwenhoven, D. vander Marel, and C. T. Foxon, Phys. Rev. Lett. **60**, 848 (1988).

[2]D. A. Wharam, T. J. Thornton, R. Newbury, M. Pepper, H. Ahmed, J. E. F. Frost, D. G. Hasko, D. C. Peacock, D. A. Ritchie, and G. A. C. Jones, J. Phys. C **21**, L209 (1988).

[3]G. Timp, A. M. Chang, P. M. Mankiewich, R. E. Behringer, J. E. Cunningham, T. Y. Chang, and R. E. Howard, Phys. Rev. Lett. **59**, 732 (1987).

[4]M. L. Roukes, A. Scherer, S. J. Allen, Jr., H. G. Craighead, R. M. Ruthen, E. D. Beebe, and J. P. Harbison, Phys. Rev. Lett. **59**, 3011 (1987).

[5]C. J. B. Ford, S. Washburn, M. Büttiker, C. M. Knoedler, and J. M. Hong, Phys. Rev. Lett. **62**, 2724 (1989).

[6]G. Timp, H. U. Baranger, P. de Vegvar, J. E. Cunningham, R. E. Howard, R. E. Behringer, and P. M. Mankiewich, Phys. Rev. Lett. **60**, 2081 (1988).

[7]Y. Takagaki, K. Gamo, S. Namba, S. Takaoka, K. Murase, S. Ishida, K. Ishibashi, and Y. Aoyagi, Solid State Commun. **68**, 1051 (1988); **69**, 811 (1989).

[8]Y. Hirayama and T. Saku, Phys. Rev. B **39**, 5535 (1989); Appl. Phys. Lett. **54**, 2556 (1989); Y. Hirayama, T. Saku, and Y. Horikoshi, Jpn. J. Appl. Phys. **28**, L701 (1989).

[9]B. J. van Wees, L. P. Kouwhenhoven, H. van Houten, C. W. J. Beenakker, J. E. Mooij, C. T. Foxon, and J. J. Harris, Phys. Rev. B **38**, 3625 (1988).

[10]D. A. Wharam, M. Pepper, H. Ahmed, J. E. F. Frost, D. G. Hasko, D. C. Peacock, D. A. Ritchie, and G. A. C. Jones, J. Phys. C **21**, L887 (1988).

[11]C. W. J. Beenakker and H. van Houten, Phys. Rev. B **39**, 10445 (1989).

[12]Y. Hirayama and T. Saku, Phys. Rev. B **41**, 2927 (1990).

[13]B. J. van Wees, L. P. Kouwenhoven, C. J. P. M. Harmans, J. G. Williamson, C. E. Timmering, M. E. I. Broekaart, C. T. Foxon, and J. J. Harris, Phys. Rev. Lett. **62**, 2523 (1989).

[14]Y. Hirai and T. Saku, Solid State Commun. **73**, 113 (1990).

[15]H. van Houten, C. W. J. Beenakker, J. G. Williamson, M. E. I. Broekaart, P. H. M. van Loosdrect, B. J. van Wees, J. E. Mooij, C. T. Foxon, and J. J. Harris, Phys. Rev. B **39**, 8556 (1989).

[16]L. W. Molenkamp, A. A. M. Staring, C. W. J. Beenakker, R. Eppenga, C. E. Timmering, J. G. Williamson, C. J. P. M. Harmans, and C. T. Foxon, Phys. Rev. B **41**, 1274 (1990).

[17]K. Nakamura, D. C. Tsui, F. Nihey, H. Toyoshima, and T. Itoh, Appl. Phys. Lett. **56**, 385 (1990).

[18]M. Okada, M. Saito, K. Kosemura, T. Nagata, H. Ishiwari, and N. Yokoyama, in Superlatt. Microstruct. (to be published).

[19]L. I. Glazman, G. B. Lesovik, D. E. Khmelnitskii, and R. I. Shekter, Pis'ma Zh. Eksp. Teor. Fiz. **48**, 218 (1988) [JETP Lett. **48**, 238 (1988).

[20]A. Yacoby and Y. Imry, Phys. Rev. B **41**, 5341 (1990).

[21]L. I. Glazman and M. Jonson, J. Phys. Condens. Matter **1**, 5547 (1989).

[22]M. C. Payne, J. Phys. Condens. Matter **1**, 4939 (1989).

[23]A. Kawabata, J. Phys. Soc. Jpn. **58**, 372 (1989).

[24]A. Szafer and A. D. Stone, Phys. Rev. Lett. **62**, 300 (1989).

[25]D. van der Marel and E. G. Haanappel, Phys. Rev. B **39**, 7811

(1989).
[26]Song He and S. Das Sarma, Phys. Rev. B **40**, 3379 (1989).
[27]G. Kirzenow, Phys. Rev. B **39**, 10452 (1989).
[28]E. Tekman and S. Ciraci, Phys. Rev. B **39**, 8772 (1989).
[29]L. Escapa and N. Garcia, J. Phys. Condens. Matter **1**, 2125 (1989).
[30]L. I. Glazman and A. V. Khaetskii, J. Phys. Condens. Matter **1**, 5005 (1989).
[31]K. B. Efetov, J. Phys. Condens. Matter **1**, 5535 (1989).
[32]H. U. Baranger and A. D. Stone, Phys. Rev. Lett. **63**, 414 (1989); Surf. Sci. **229**, 212 (1990).
[33]H. Akera and T. Ando, Surf. Sci. **229**, 268 (1990); Phys. Rev. B **41**, 11 967 (1990).
[34]D. S. Fisher and P. A. Lee, Phys. Rev. B **23**, 6851 (1981).
[35]A. D. Stone and A. Szafer, IBM J. Res. Dev. **32**, 384 (1988).
[36]H. U. Baranger and A. D. Stone, Phys. Rev. B **40**, 8169 (1989).
[37]R. Landauer, IBM J. Res. Dev. **1**, 223 (1957); Philos. Mag. **21**, 863 (1970).
[38]P. A. Lee and D. S. Fisher, Phys. Rev. Lett. **47**, 882 (1981).
[39]D. J. Thouless and S. Kirkpatrick, J. Phys. C **14**, 235 (1981).
[40]A. MacKinnon and B. Kramer, Phys. Rev. Lett. **47**, 1546 (1981); **49**, 695 (1982); Z. Phys. B **53**, 1 (1983).
[41]J. L. Pichard and G. Sarma, J. Phys. C **14**, L127 and L617 (1981).
[42]C. M. Soukoulis, I. Webman, C. S. Grest, and E. N. Economou, Phys. Rev. B **26**, 1838 (1982); A. C. Zdetsis, C. M. Soukoulis, E. N. Economou, and G. S. Grest, *ibid.* **32**, 8711 (1985); C. M. Soukoulis, A. D. Zdetsis, and E. N. Economou, *ibid.* **34**, 2253 (1986).
[43]L. Schweitzer, B. Kramer, and A. MacKinnon, J. Phys. C **17**, 4111 (1984); A. MacKinnon, L. Schweitzer, and B. Kramer, Surf. Sci. **142**, 189 (1984); B. Bulka, M. Schreiber, and B. Kramer, Z. Phys. B **66**, 21 (1987).
[44]T. Ando and H. Aoki, J. Phys. Soc. Jpn. **54**, 2238 (1985); H. Aoki and T. Ando, Phys. Rev. Lett. **54**, 831 (1985).
[45]T. Ando, Phys. Rev. B **40**, 5325 (1989); **42**, 5626 (1990).
[46]A. MacKinnon, Z. Phys. B **59**, 385 (1985).
[47]R. A. Jalabert, H. U. Baranger, and A. D. Stone, Phys. Rev. Lett. **65**, 2442 (1990).